Rock Mechanics and Rock Engineering
https://doi.org/10.1007/s00603-024-03787-9

ORIGINAL PAPER

Rock Mass Structure Characterization Considering Finite and Folded Discontinuities: A Parametric Study

Georg H. Erharter[1,2]

Received: 21 August 2023 / Accepted: 17 January 2024

Abstract

The quantification of a rock mass's internal structure and description of discontinuity properties is imperative for modern rock mass characterization. This study builds on decades of rock engineering development by reviewing and revising different parameters such as the rock quality designation (RQD), volumetric joint count (J_v), the Pij system and others. Analyses of these parameters are done by means of a Monte Carlo simulation that generated 5000 samples of discrete discontinuity networks including finite, folded and very low to very high discontinuity densities (J_v range: 0.5–117 discontinuities/m^3), thus representing a wide range of possible geological scenarios. *P*10, *P*20, *P*21, *P*30, *P*32, *RQD* and the fractal dimension of the rock mass are virtually measured on these samples and a range of higher level parameters that are used in practical rock engineering computed and their relationships investigated. It is concluded that parameters which are based on subjective estimations of discontinuity spacing, the number of discontinuity sets or *RQD* are not suited to describe the rock mass structure in cases of demanding geological scenarios featuring many discontinuities, weak and anisotropic rock masses, metamorphic rock masses, folded rock masses, etc. By revising classical parameters and their relationships, this study contributes to basic rock mass characterization and furthermore paves the way for future developments by making the developed discrete discontinuity network dataset and all included codes openly accessible to the rock mechanics community.

Highlights

- This study contributes to rock mass characterization by reviewing classical parameters based on simulated discrete discontinuity networks.
- A dataset of 5000 simulated discrete discontinuity networks including a vast variety of geological scenarios is built.
- Parameters based on numbers of discontinuity sets, discontinuity spacing and the RQD are not suited to describe complex rock mass conditions.
- The dataset and code of the study is provided openly to enable future advancements in rock mechanics.

Keywords Rock mass · Characterization · Discrete fracture network · Monte Carlo simulation · Parameter determination

1 Introduction

"Every rock, without exception, has more or less conspicuous mechanical defects which have no direct connection with its inherent properties", was already stated by Terzaghi (1946)—chapter 2—in his foundational work on "Rock Defects and Loads on Tunnel Supports". It was recognized early in rock engineering that a distinction between "intact rock" and "rock mass" is necessary and the difference from the former to the latter is the consideration of discontinuities

✉ Georg H. Erharter
georg.erharter@ngi.no

[1] Norwegian Geotechnical Institute, Sandakerveien 140, Oslo, Norway

[2] Institute of Rock Mechanics and Tunnelling, Graz University of Technology, Rechbauerstraße 12, Graz, Austria

Published online: 19 March 2024

Table 1 Definition of the measures for discontinuity density modified after Dershowitz and Herda (1992)

P_{ij} notation	Definition
$P10$	Number of discontinuities per unit length of borehole/scan line
$P20$	Number of discontinuities per unit area
$P21$	Length of discontinuities per unit area
$P30/J_v$	Number of discontinuities per unit volume
$P32$	Area of discontinuities per unit volume

and other phenomena (e.g., weathering) that modify the original rock's properties. Discontinuities within rock are products of its geological history and/or created through anthropogenic influences (e.g., blasting) and make up the overall rock mass structure. Consequently, characterization of the rock mass structure is imperative for rock engineering, and over the past decades, engineers developed a plethora of methods to put numbers to this geological feature (Hoek 1999). Several methods of rock mass structure characterization are furthermore directly included within rock engineering design schemes.

The rock quality designation (RQD) from Deere (1964) is one of the oldest parameters to quantify the discontinuity density in rock masses, finds direct application in the Q-system (Barton et al. 1974) and the Rock Mass Rating (RMR) (Bieniawski 1973) and is still part of today's international standard of rock characterization: ISO 14689. Today, however, the value and validity of RQD is questioned due to deficits such as inconsistent definitions, subjectivity, biased data acquisition, susceptibility to orientation, etc. (Pells et al. 2017). The *Pij* system by Dershowitz and Herda (1992) presents a more holistic approach to discontinuity density quantification and includes all possible measuring dimensions (1D, 2D, 3D) versus different dimensionalities of discontinuity-geometry properties (count, length, volume). The volumetric joint count (J_v) was developed by Palmstrøm (1974) in parallel to the development of the Rock Mass index (RMi) (Palmstrøm 1995, 1996) as a means to quantify the volumetric discontinuity density. J_v, therefore, corresponds to $P30$ by Dershowitz and Herda (1992) (see Table 1 for *Pij* definitions). The mentioned parameters for rock mass structure quantification are among the most popular that are in use today and over the decades also several attempts towards establishing relationships between the parameters were made (e.g., Palmstrøm (2005); Zhang (2016); Zheng et al. (2020)).

However, several of the mentioned parameters as well as the relationships between each other suffer from two problems: (i) the used data to develop the parameter insufficiently covers the state space (e.g., only data from one kind of rock mass was used); (ii) the development was done under simplifying assumptions such as perfectly planar discontinuities, infinitely extended discontinuities, non-variable discontinuity orientations, and low discontinuity densities. Even though these problems are justifiable for the individual studies, where the first one is usually related to limited access to data and the second one to limited computational power at the time of development, they do pose problems when it comes to how realistic the parameters and their relationships are.

Based on today's easy access to computational power, this work contributes to basic rock mass characterization by adding new insights to the quantification of a rock mass's structure and, therefore, continues the fundamental work of the above-mentioned authors. For this purpose, a whole range of parameters for rock mass characterization are investigated based on a Monte Carlo simulation with 5000 generated 3D discrete discontinuity networks (i.e., discrete fracture network (DFN), but the author refrains from terminology that unjustifiably implies the geological genesis of a discontinuity—see below). The simulation is set up in a way that an extremely broad range of possible rock mass structures is generated including finite and folded discontinuities and massive to crushed rock masses. While these features of the simulation already distinguish this contribution from other recent studies based on 3D discrete fracture networks (e.g., Gómez et al. (2023); Ojeda et al. (2023); Xiao et al. (2023); Zhang et al. (2022)), this study also investigates advanced parameters of rock mass characterization such as the fractal dimension of the generated samples. Lastly, the generated dataset (termed: parametric discontinuity dataset 1—PDD1) including the code for the analysis and the derived and computed parameters are made openly available for the rock mechanics community for the sake of complete transparency and as a base for further developments (see data availability statement).

In this paper, the definition of a "discontinuity" of ISO 14689 is used: "break in the rock material continuity that is open or can open under the stress increase or reduction as a result of the engineering works". This definition is chosen since it is not specific for the geological genesis of a discontinuity in rock and thus also includes joints, fractures, faults, bedding planes, schistosity-/foliation planes or slickensides. Using specific discontinuity types synonymously for all discontinuities is seen as a confusing, non-conducive terminological practice that should be avoided.

In Sect. 2, PDD1, its generation, virtually measured as well as computed parameters are presented. Section 3 elaborates relationships between virtually measured parameters of PDD1 and Sect. 4 discusses the study's findings. In the outlook of Sect. 5, current and possible future developments are pointed out which can be based on PDD1.

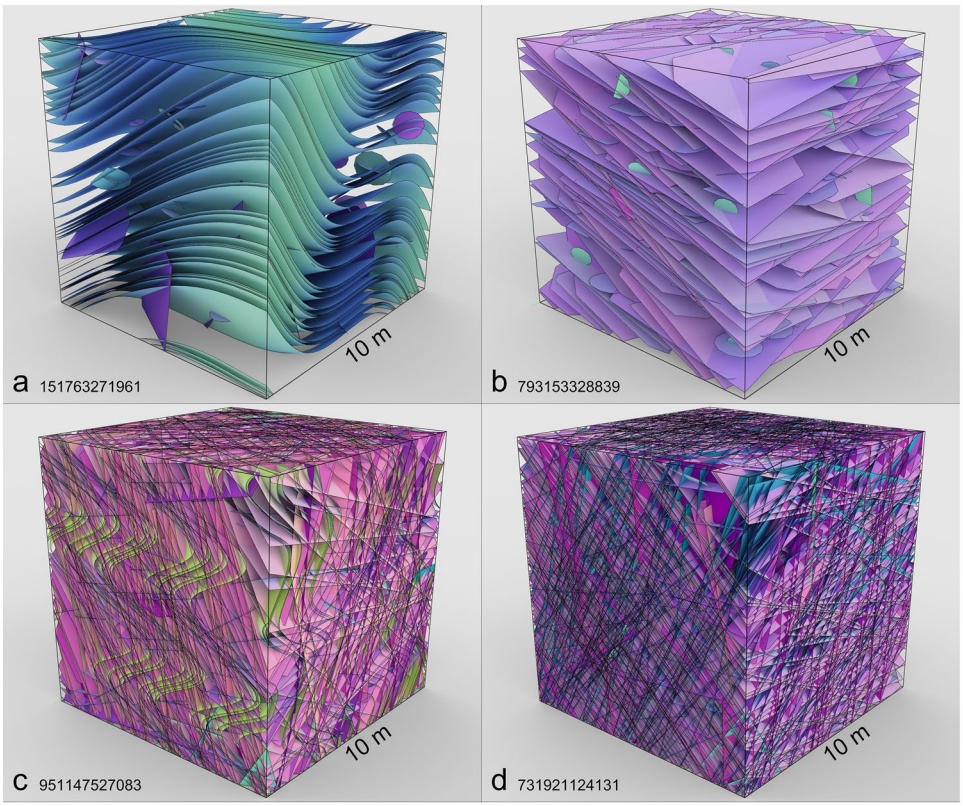

Fig. 1 Examples showing the variety of PDD1 with discontinuities colored according to their orientation (sample IDs are given in lower left corners of subplots). **a** folded rock mass with low discontinuity density; **b** rock mass with planar discontinuities and one dominant set with preferred orientation; **c** rock mass with a high density of both folded and planar discontinuities; **d** rock mass that is heavily intersected by discontinuities. Cross-sections through the samples are given in Fig. 10a–d

2 Parametric Discontinuity Dataset

This section elaborates the generation of PDD1, virtual measurements that were taken on it and computed parameters. A description of all input-, virtually measured- and computed parameters of the dataset is given in Table 5 in the Appendix of the paper. PDD1—which can be downloaded from the GitHub repository provided under the data availability statement of this paper—also contains a list of all samples including the exact input parameters that permit reproduction of the measured and computed output parameters.

2.1 Dataset Generation

The dataset was generated using the "Grasshopper" environment inside the general purpose "Rhinoceros 3D" v.7. computer-aided design (CAD) software (Robert McNeel & Associates 2023). Grasshopper is a visual programming language that is made for parametric modeling of geometries and information. In contrast to explicit CAD modeling, where geometries and information are created and manipulated manually, in parametric design, the modeling is done based on algorithms and parameters. Model updates with new parameters are, therefore, easy to implement and do not require manual redrawing. This capability makes Grasshopper well suited for large-scale parametric studies such as presented in this paper. Advantages over commercially available DFN modeling software are that Grasshopper gives the user (i) full control over the input and output of a parametric study, (ii) full control over the modeled geometry (e.g., capability of modeling folded surfaces is often very limited in DFN software), (iii) the capability to parallelize the computation of processes to a certain extent, (iv) the ability to use Rhino's general purpose CAD functions for post processing of models (e.g., rendering—see Fig. 1). The Grasshopper scripts for dataset generation and reproduction of samples can be found in the GitHub repository provided under the data availability statement of the paper.

Each sample in the dataset consists of discontinuities that are generated within a square bounding box of 10 m edge length. This size was chosen as a tradeoff between computational performance (some virtual measurements are very demanding; e.g., volumetric joint count or fractal dimension—see next section) and achieving a representative volume size for many rock engineering applications while also modeling high discontinuity densities (up to a volumetric joint count of 117 discontinuities per m^3).

The discontinuities of each sample are generated based on four theoretical discontinuity sets: (i) set 1 can consist either of finite and planar discontinuities with a defined orientation or folded and through-going discontinuities (randomly chosen); (ii) set 2 and 3 consist of finite and planar

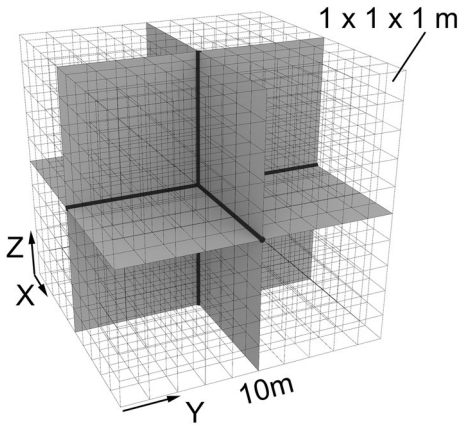

Fig. 2 Virtual measuring devices to retrieve 1D- (black lines), 2D- (grey planes) or 3D parameters (transparent boxes)

discontinuities with a defined orientation; (iii) set 4 consists of finite and planar discontinuities with random orientation which have a smaller size than the other discontinuity sets (Twiss and Moores 2007). Finite and planar discontinuities are modeled with 12-sided polygons since this is computationally advantageous for intersections in comparison to "real" circles. The four discontinuity sets are called "theoretical" since their actual degree of occurrence in the rock mass sample depends on several input parameters (i.e., number of discontinuities per set, size, size variation, variation of orientation). Consequently, a discontinuity set may be generated, but it is hardly observable in the sample due to high variations of orientation, small sizes or a low number of discontinuity planes. This generation method allows to create a wide variety of rock mass structures ranging from rock masses with few, small, random discontinuities, rock masses with pronounced folding to rock masses with several well-defined discontinuity sets (see examples in Fig. 1). Statistical properties of the input parameters for the modeling are given separately for samples with planar discontinuities only (Table 6) and samples with both folded and planar discontinuities (Table 7) in the Appendix.

2.2 Virtual Measurements of Rock Mass Structure

To retrieve virtual measurements of linear, areal, or volumetric discontinuity properties (see below), different virtual measuring devices are implemented (Fig. 2). 1D parameters (e.g., RQD, $P10$) are measured in three perpendicular directions along measuring lines parallel to the global X, Y, and Z axes which intersect in a sample's center. 2D parameters (e.g., $P20$, $P21$) are measured on three planes perpendicular to the global X, Y and Z axes that are centered in the sample. 3D parameters (e.g., $P30/J_v$, $P32$) are measured with

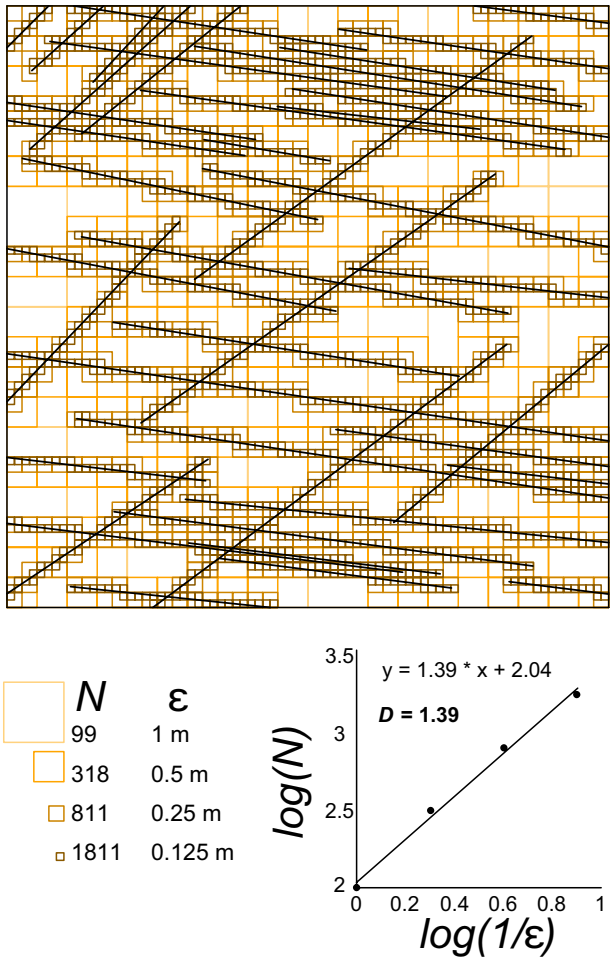

Fig. 3 Generic example for how the "box counting dimension" can be computed for a 2D discontinuity network. N denotes the number of required boxes and ϵ the box edge lengths. The shown network has a fractal dimension of 1.39

respect to 1000 cubes of 1 m side length that completely fill the sample volume.

The following measurements were taken virtually for each sample in PDD1: (i) linear measurements of the RQD (as defined in ISO 14689), the $P10$ value and the apparent discontinuity spacing, all measured in X, Y, Z directions of the sample; (ii) measurements of $P20$ and $P21$ in three planes perpendicular to the X, Y and Z directions; (iii) volumetric measurements of $P30/J_v$ and $P32$. The Pij measurements were first introduced by Dershowitz and Herda (1992) and describe the dimension of the measurement region (i: 1 = line, 2 = plane, 3 = volume) vs. the dimension of the discontinuity measure (j; 0 = count, 1 = length, 2 = area, 3 = volume). Note that Dershowitz and Herda (1992) start j with 1 = count, but this has been changed to 0 in several publications (e.g., Rogers et al.

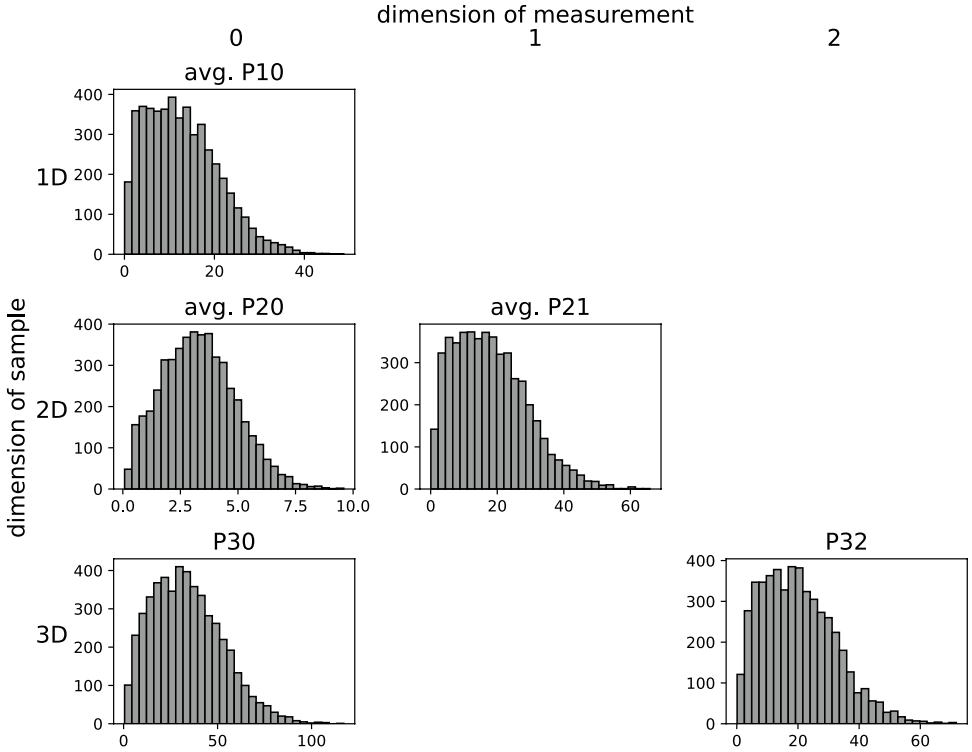

Fig. 4 Histograms of the average $P10$, average $P20$, average $P21$, $P30/J_v$ and $P32$ measurements of the dataset. For more information on the Pij system, see Dershowitz and Herda (1992) or e.g., Rogers et al. (2017)

(2017)) since the discontinuity count is dimensionless. This paper also follows this system and the adopted definition of the Pij system is given in Table 1.

$P11$, $P22$ and $P33$ would require discontinuity models with a volume which was out of scope for PDD1. The "apparent spacing" is defined as the average length of the pieces of a measuring line that gets intersected by all discontinuities of the sample. The spacing of each discontinuity set is measured with a measuring profile that is perpendicular to the average discontinuity set orientation, respectively perpendicular to the base planes of a folded discontinuity set. In both cases—planar finite discontinuities and folded discontinuities—geometrical issues arise: in the case of planar, finite discontinuity sets, discontinuities that do not intersect the measuring line, do not contribute to the computation of the spacing. In the case of folded discontinuity sets, the spacing is affected by different distances between the folded planes in the case of non-parallel folds. This way of discontinuity spacing measurement was chosen as it produces consistent measurement and the spacing is required to compute different versions of J_v (Eqs. 2, 3, 6; see next section). In many cases, however, discontinuity spacing is seen as an ill-defined parameter and a discussion on it can be found in Sect. 4 (Fig. 10). For each of the four theoretical discontinuity sets, the total area of the discontinuities is also measured.

The fractal dimension (D) for the samples of PDD1 was assessed in 3D, in a similar way as $P30/J_v$ and $P32$ were measured through intersecting virtual boxes with discontinuities. The fractal dimension of a geometry can be seen as a parameter for the geometry's complexity (in this case for the discontinuity density) and is usually a value in between the dimensions: 1, 2, 3. Fractal dimensions have been used extensively in geoscientific literature decades ago to characterize different properties of discontinuities based on 1D scanlines (e.g., Boadu and Long (1994); Lee et al. (1990)) or 2D fracture trace maps (e.g., Berkowitz and Hadad (1997); Roy et al. (2007)).

The fractal dimension of each sample was measured using the Minkowski–Bouligand dimension—also known as "box counting dimension". For that, each samples' discontinuities were intersected four times with boxes of decreasing size where box edge lengths (ε) of 0.25, 0.125, 0.0625, 0.03125 m are used and the number of intersected boxes (N) is recorded. D is then computed from the slope of a linear regression that is fitted to the points resulting from Eq. 1 for each pair of N and ε:

$$D = \lim_{\varepsilon \to 0} \frac{\log N(\varepsilon)}{\log 1/\varepsilon} \tag{1}$$

Figure 3 shows a generic 2D example for how to measure the fractal dimension for a 2D discontinuity trace map with comparably large box edge lengths for visual purposes. Measuring D in 3D works in the same way with the only difference that instead of 2D boxes, 3D boxes are used, and the box edge lengths are smaller than in the

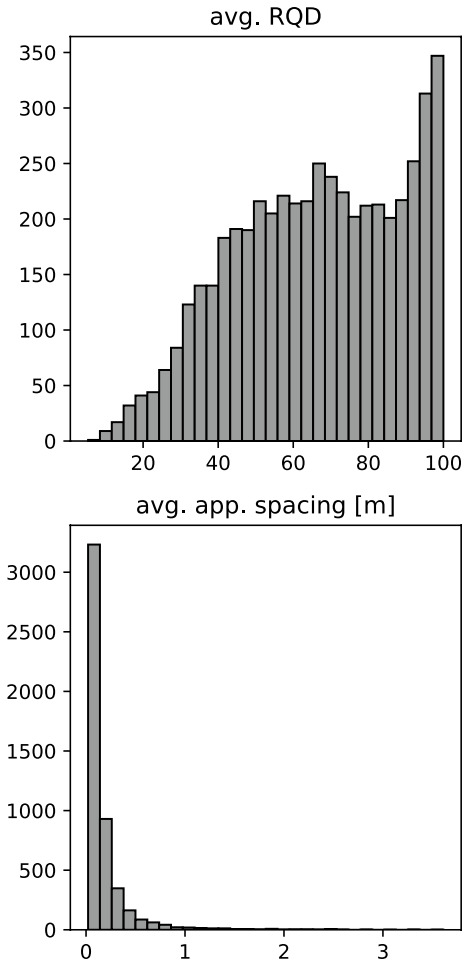

Fig. 5 Histograms for the average RQD and average apparent spacing of the dataset

shown example. The majority of measured fractal dimensions of the samples is between 2D and 3D although there are samples with a D as low as 1.6. D generally increases with $P10$, $P20$, $P21$, $P30/J_v$ and $P32$, and decreases with RQD (see Sect. 3 and Fig. 11).

Statistical properties of the measured parameters of PDD1 can be found in Table 8 in the Appendix of the paper.

2.3 Computed Parameters of Rock Mass Structure

Based on the virtually measured parameters, a whole range of additional rock mass parameters are computed. For the directionally dependent measures RQD, $P10$, $P20$, $P21$ and the apparent spacing, average values are computed. Histograms for the Pij discontinuity density measures of PDD1 are given in Fig. 4 and for RQD and the average apparent spacing in Fig. 5. $P10$, $P20$, $P21$, RQD and the apparent spacing are average values over their respective three directions.

The volumetric joint count (J_v, i.e., the number of discontinuities per unit volume of 1 m^3 of rock mass) is computed using 5 equations from different authors which are denoted as J_{v1} to J_{v5}. Acc. to ISO 14689 and originally based on Palmstrøm (1982), J_v can be computed with Eq. 2 where $s1$, $s2$ and $s3$ are the discontinuity spacings of set 1, 2 and 3, respectively:

$$J_{v1} = \frac{1}{s1} + \frac{1}{s2} + \frac{1}{s3} \tag{2}$$

Palmstrøm (2000) then presented a revised version of Eq. 2: Eq. 3. There the original formulation has been extended to also include more than three discontinuity sets and a term for random discontinuities where Nr is the number of random discontinuities and the denominator of 5 is a recommended spacing for random discontinuities based on the author's experience. In this study, $Nr = 1$ was used to account for random discontinuities:

$$J_{v2} = \frac{1}{s1} + \frac{1}{s2} + \frac{1}{s3} + \cdots + \frac{Nr}{5} \tag{3}$$

Sonmez and Ulusay (1999) presented two new relationships to estimate J_v: (i) Eq. 4 computes J_{v3} as the product of the number of discontinuity intersections (N_x, N_y, N_z) of three perpendicular scanlines with lengths L_x, L_y, L_z, which is equivalent to the definition of $P10$ (see Table 1). Since PDD1 contains three perpendicular measurements of $P10$ for every sample, in this study $J_{v3} = P10x \times P10y \times P10z$ is used. In homogeneous cases, Sonmez and Ulusay (1999) then further proposed to rewrite Eq. 4 to Eq. 5 where N and L are the numbers of discontinuity intersections and the length of one single scanline respectively where herein the average $P10$ was used:

$$J_{v3} = \frac{N_x}{L_x} \times \frac{N_y}{L_y} \times \frac{N_z}{L_z} \tag{4}$$

Table 2 Rule set to determine the number of discontinuities in a sample

Number of discontinuity sets D_n	Rule
0	If measured $J_v < 1$ (based on Ulusay and Hudson (2007))
4	If 4/4 sets have an area ratio of > 15% of the total discontinuity area each
3	If 3/4 sets have an area ratio of > 20% of the total discontinuity area each
2	If 2/4 sets have an area ratio of > 22.5% of the total discontinuity area each
1	If 1/4 sets has an area ratio of > 40% of the total discontinuity area

Table 3 Rule set to determine the Q-system's "joint set number" of a sample

Joint set number J_n	Rule
1	If measured $J_v < 1$ (based on Ulusay and Hudson (2007))
20	If measured $J_v > 60$ (based on Ulusay and Hudson (2007))
15	If 4/4 sets have an area ratio of > 15% of the total discontinuity area each and measured J_v is > 30
12	If 4/4 sets have an area ratio of > 15% of the total discontinuity area each
9	If sets 1–3 have an area ratio of > 20% of the total discontinuity area each
6	If the random set 4 and either sets 1 and 2, 1 and 3 or 2 and 3 have an area ratio of > 20% of the total discontinuity area
4	If 2 of sets 1–3 have an area ratio of > 25% of the total discontinuity area each
3	If 1 of sets 1–3 and the random set 4 have an area ratio of > 30% of the total discontinuity area each
2	If 1 of sets 1–3 has an area ratio of > 40% of the total discontinuity area each

Table 4 Investigated relationships between parameters and developed functions

X	Y	Equation		R^2	Type
avg. P10	avg. P21	$P21 = 1.349 \times P10 + 0.563$	Eq. 8	0.99	li
avg. P10	J_v measured	$J_v = 2.313 \times P10 + 3.978$	Eq. 9	0.99	li
avg. P10	P32	$P32 = 1.47 \times P10 + 1.226$	Eq. 10	0.97	li
avg. P21	J_v measured	$J_v = 1.71 \times P21 + 3.105$	Eq. 11	0.99	li
avg. P21	P32	$P32 = 1.097 \times P21 + 0.483$	Eq. 12	0.99	li
P32	J_v measured	$J_v = 1.548 \times P32 + 2.571$	Eq. 13	0.98	li
avg. P10	avg. P20	$P20 = 0.555 \times P10^{0.713}$	Eq. 14	0.93	po
avg. P10	Fractal dimension	$D = 1.844 \times P10^{0.115}$	Eq. 15	0.79	po
avg. P20	avg. P21	$P21 = 3.901 \times P20^{1.25}$	Eq. 16	0.93	po
avg. P20	P32	$P32 = 4.591 \times P20^{1.215}$	Eq. 17	0.92	po
avg. P20	J_v measured	$J_v = 8.386 \times P20^{1.151}$	Eq. 18	0.96	po
avg. P20	Fractal dimension	$D = -2.049 \times P20^{0.153}$	Eq. 19	0.76	po
avg. P21	Fractal dimension	$D = 1.741 \times P21^{0.122}$	Eq. 20	0.82	po
P32	Fractal dimension	$D = 1.69 \times P32^{0.127}$	Eq. 21	0.83	po
J_v measured	Fractal dimension	$D = 1.523 \times J_v^{0.137}$	Eq. 22	0.80	po
avg. RQD	Fractal dimension	$D = -2.1^{-7} \times RQD^{3.3} + 2.75$	Eq. 23	0.72	po
avg. P10	avg. RQD	$RQD = 100e^{-0.1 \times P10} \times (0.1 * P10 + 1)$	Eq. 24	0.97	ex
avg. P20	avg. RQD	$RQD = 100e^{-0.38 \times P20} \times (0.38 \times P20 + 1)$	Eq. 25	0.90	ex
avg. P21	avg. RQD	$RQD = 100e^{-0.07 \times P21} \times (0.07 \times P21 + 1)$	Eq. 26	0.96	ex
P32	avg. RQD	$RQD = 100e^{-0.06 \times P32} \times (0.06 \times P32 + 1)$	Eq. 27	0.94	ex
J_v measured	avg. RQD	$RQD = 100e^{-0.037 \times J_v} \times (0.037 \times J_v + 1)$	Eq. 28	0.97	ex

li linear, *po* power law, *ex* exponential

$$J_{v4} = \left(\frac{N}{L}\right)^3 \tag{5}$$

With the overall average discontinuity spacing (S), another way of computing J_v was presented by Sönmez and Ulusay (2002) where D_n is the estimated number of discontinuity sets (Eq. 6):

$$J_{v5} = D_n\left(\frac{1}{S}\right) \tag{6}$$

As stated in Sect. 2.1, the number of discontinuity sets is highly variable in PDD1 and cannot be directly derived from the input. To determine D_n, the ratio of the total measured discontinuity area of each of the four sets with respect to the total discontinuity area of all sets was computed. The measured discontinuity area of a set is seen as most representative for how much this set actually contributes to the overall rock mass structure. In reality, this observation cannot be made, and the number of discontinuity sets is usually visually estimated by the geotechnical engineer. A discussion about which problems arise with this approach is given in Sect. 4. Nevertheless, the discontinuity area ratios were then used to estimate the number of discontinuity sets following

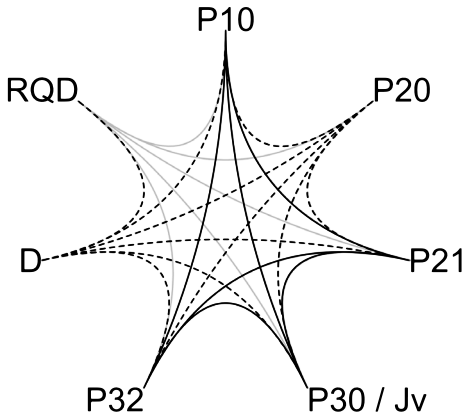

Fig. 6 Relationship types that were identified between the seven measured parameters. Through-going black line: linear relationship; dashed black line: power law; grey line: exponential

the rules in Table 2. The thresholds were defined by trial and error and comparing different discontinuity associations.

The first term of the Q-system, i.e., RQD/J_n (Barton et al. 1974), which should describe the rock mass' structure was also computed and investigated. Whereas the required RQD in RQD/J_n can be estimated for samples of PDD1 by the average RQD (see, e.g., Fig. 5), the "joint set number" J_n must be determined in a similar manner as D_n (Table 2) but it cannot be done in the same way since the Q-system differentiates between random and non-random discontinuity sets. The rule set to determine J_n is given in Table 3.

The average block volume (V_b) is computed according to Palmstrøm (2000) with Eq. 7 where α, β and γ are the angles between discontinuity set 1 and 2, 2 and 3 and 1 and 3, respectively, that were computed based on the planes' normals. V_b cannot be computed for samples with a folded discontinuity set because of the geometrical impossibility to compute the angle between folded and planar planes:

$$V_b = s1 \times s2 \times s3 \times (sin(\alpha) \times sin(\beta) \times sin(\gamma)) \quad (7)$$

Statistical properties of the computed parameters of PDD1 can be found in Table 9 in the Appendix of the paper.

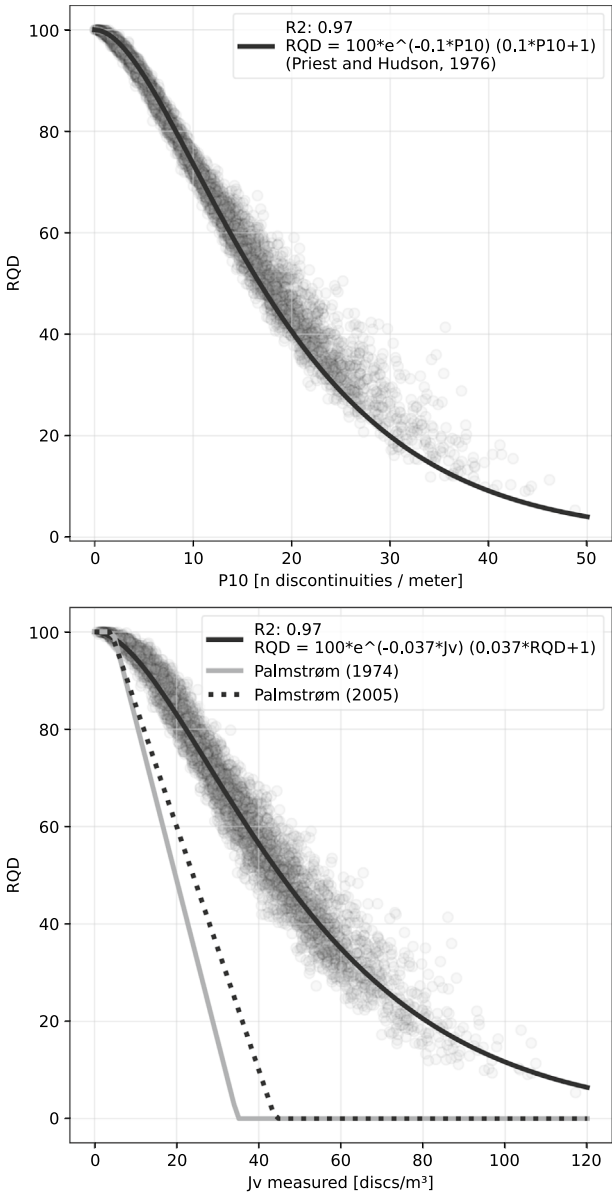

Fig. 7 Top: $P10$ vs. RQD of PDD1 in a scatterplot and the perfectly fitting relationship by Priest and Hudson (1976) as a bold black line; Bottom: J_v vs. RQD including the linear relationships proposed by Palmstrøm (1974, 2005) and the new exponential relationship as proposed herein

3 Investigated Relationships

The following measured parameters of PDD1 were closer investigated with respect to relations to each other: avg. RQD, avg. $P10$, avg. $P20$, avg. $P21$, $P30/J_v$, $P32$, and the fractal dimension acc. to Minkowski–Bouligand. Correlating measured parameters and highly computed parameters such as the computed block volume was not done due to the inherent uncertainty and model bias of these parameters. Plotting the measured parameters against each other shows that their relationships can be well approximated with either linear-, power law, or exponential functions. The goodness of fit was assessed with the coefficient of determination (R^2) where an R^2 of 1 indicates a perfect fit and the metric can become infinitely negative in case of poor fits. The developed relationships are given in Table 4 and visualized in the pairplot of Fig. 11 in the appendix of the paper.

The linear relationships all achieve high R^2 values > 0.97 and are seen as good fits. It can be observed that while all relationships between $P10$, $P21$, $P30$ and $P32$ are linear,

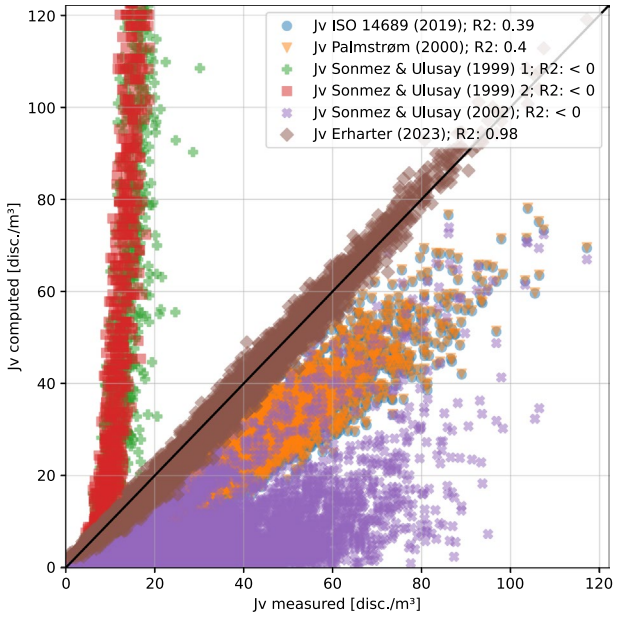

Fig. 8 Relationships between different proposals of how to compute the volumetric joint count vs. the virtually measured volumetric joint count of PDD1

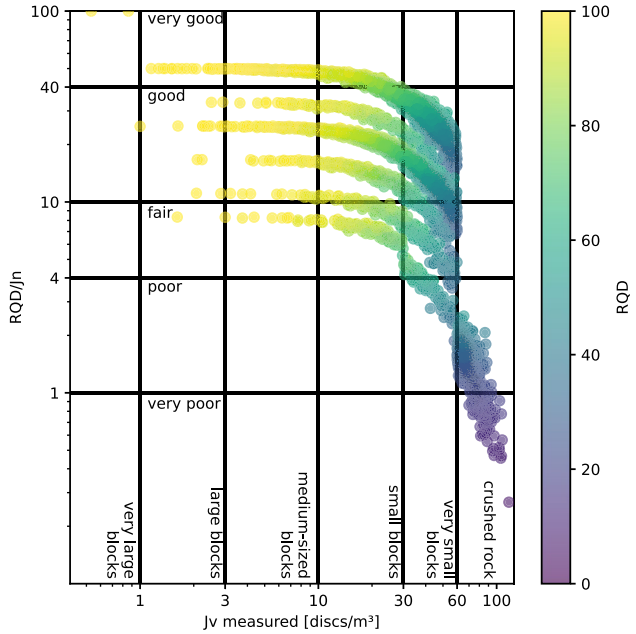

Fig. 9 The relationship between the rock mass structural term of the Q-system (i.e., RQD/J_n), the volumetric joint count and the *RQD*

the relationship between these parameters and *P*20 is non-linear and is, therefore, fitted with a power-law function. All relationships to the fractal dimension *D* can be described with power-law functions as well although lower R^2 values between 0.72 and 0.83 are achieved due to the larger

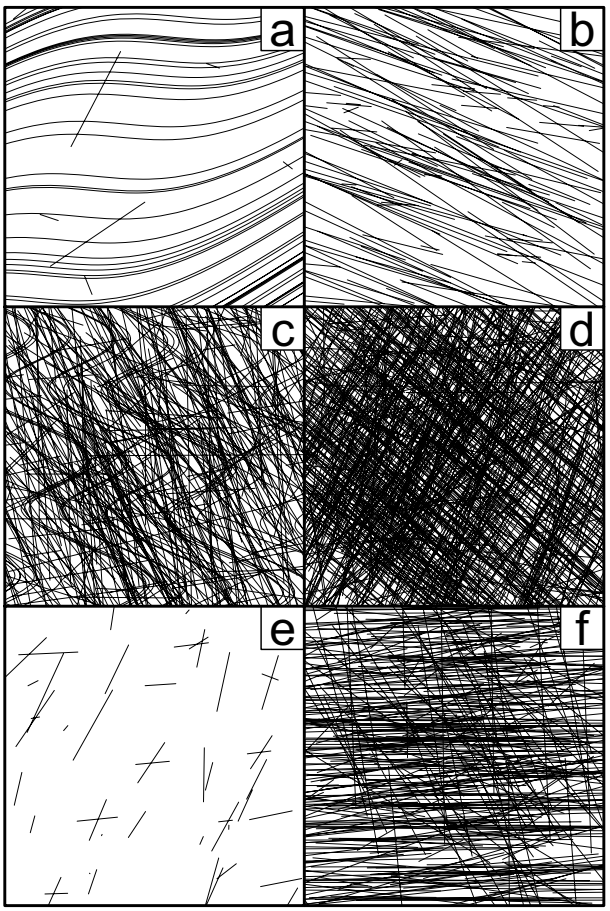

Fig. 10 Exemplary 2D sections through samples of PDD1 to illustrate the challenge of assessing discontinuity sets based discontinuity spacings. The sample IDs are: **a** 151763271961, **b** 793153328839, **c** 951147527083, **d** 731921124131, **e** 413944382633, **f** 111446083430. Note that samples a–d are the same as in Fig. 1

variability in *D*. The relationship between RQD and *D* is the only one that requires a negative power-law function. All other relationships with RQD are well represented with an exponential function of the type of function that was developed by Priest and Hudson (1976) (Eq. 29). In Eq. 29 (i.e., eq. 4 in Priest and Hudson (1976)), λ represents the mean number of discontinuities per meter of scanline which matches the definition of *P*10 (see Table 1) and *t* represents a "threshold value" which Priest and Hudson (1976) recommends to be set to 0.1. This is the same as Eq. 24 (i.e., Eq. 5 in Priest and Hudson (1976)) which is a perfect fit for the data of PDD1 with an R^2 of 0.97 (Fig. 7, top):

$$RQD = 100e^{-\lambda \times t} \times (\lambda \times t + 1) \tag{29}$$

If λ in Eq. 29 is replaced with *P*20, *P*21, *P*32 or $P30/J_v$, only the threshold value *t* must be adjusted to retrieve good fits to *RQD* (i.e., Eqs. 25–28). Figure 6 gives a graphical representation of how the different parameter relationships

show preferred types for the individual parameters (e.g., RQD: mostly exponential and $P20$: mostly power law). Further research is required to investigate why this preference of relationship types between parameters occurs.

The relationship between RQD and J_v of Eq. 28 achieves an R^2 of 0.97. Palmstrøm (1974) already proposed a linear relationship between these parameters which he later revised to Eq. 30 (Palmstrøm 2005). In comparison to the herein proposed Eq. 28, the relationships between RQD and J_v as proposed by Palmstrøm seem to generally underestimate the RQD and might, therefore, lead to conservative estimations of the discontinuity density in rock masses (Fig. 7, bottom):

$$\mathrm{RQD} = \begin{cases} 100 \text{ for } J_v < 4, \\ 110 - 2.5J_v \text{ for } 4 < J_v < 44, \\ 0 \text{ for } J_v \geq 44 \end{cases} \tag{30}$$

As given in the previous section, J_v was computed in five different ways for the rock mass samples of PDD1. The validity of these five methods (J_{v1-5}, see Eqs. 2–6) can be assessed against the virtually measured J_v which represents the ground truth for this dataset. Both J_{v1} (Eq. 2) according to ISO 14689 based on Palmstrøm (1982) and J_{v2} (Eq. 3) according to Palmstrøm (2000) achieve R^2 values of 0.39 and 0.4, respectively. The spread of J_{v1} and J_{v2} is not too large, however, the equations generally underestimate the number of occurring discontinuities. J_{v3} (Eq. 4) and J_{v4} (Eq. 5) based on Sonmez and Ulusay (1999) vastly overestimate the number of occurring discontinuities and achieve R^2 scores far below 0. J_{v5} (Eq. 6) based on Sönmez and Ulusay (2002) computes J_v again in a similar manner as Palmstrøm (1982) but underestimates the number of discontinuities even more than J_{v1} and J_{v2} and also achieves an R^2 of <0.

Based on the experiences of this study, the author proposes a new relationship to estimate J_v which is given in Eq. 31 and achieves an R^2 of 0.98. The equation is based on the linear relationship between $P10$ and J_v as elaborated above. $P10_{\mathrm{avg}}$ should be computed as the average value of $P10$ measured in three perpendicular directions. On most rock exposures, at least two directions should be measurable and the third can be estimated, although all three directions should be measured wherever possible:

$$J_v = 3 \times P10_{\mathrm{avg}} \times 0.8 + 2 \tag{31}$$

Figure 8 shows the relationships between the measured J_v and the different computed J_v.

Lastly, the relationship between RQD/J_n and the measured J_v is investigated and shown in Fig. 9. The classification of Q-classes follows Barton et al. (1974) and the classification of J_v into block sizes follows Ulusay and Hudson (2007). In this rock mass structure focused study, the Q-classes are assigned only based on RQD/J_n which can be done if all other values of the Q-system are set to 1, thus assuming no influence of the discontinuity friction, active stresses, or water. Note that also Palmstrøm (2005) includes a classification of J_v with the same class boundaries as Ulusay and Hudson (2007) but uses the "degree of jointing" instead of "block sizes" with the following classes: very low, low, moderate, high, very high, crushed.

Figure 9 shows that while the overall relationship between RQD/J_n and J_v is qualitatively comprehensible (high RQD/J_n = low J_v and vice versa), the individual Q-classes contain a vast range of discontinuity densities. For example, "very good" rock mass conditions according to the Q-system with a $\mathrm{RQD}/J_n > 40$ can have a J_v of up to 30 corresponding to "small blocks"/"high degree of jointing". J_v values between 30 and 60 can even result in a "good" rock mass classification based on RQD/J_n. Conversely, samples with a $\mathrm{RQD} > 80$ and $J_v < 3$ are scattered across the Q-classes between very good and fair, due to the influence of the estimated number of discontinuity sets J_n. With $J_v > 60$, a rock mass classification based on a RQD/J_n would be "poor" or "very poor", thus corresponding better to the J_v classification. It must be pointed out that while the exact datapoint location of Fig. 9 is dependent on the defined J_n-thresholds of Table 3, the general patterns with large datapoint scattering and clustering of points would remain the same even if these thresholds are modified (a discussion of the patterns in Fig. 9 is given in Sect. 4).

4 Discussion

This study investigated basic parameters of rock mass structure by means of a Monte Carlo simulation of samples of finite and folded discrete discontinuities that are designed to be as realistic as possible, given the current computational possibilities. Parameters such as J_v—which are not directly observable in reality—can be directly measured in the samples which permits reassessment of other analytical ways to derive these parameters.

Computing the volumetric joint count by means of J_{v1} (Eq. 2), J_{v2} (Eq. 3) and J_{v5} (Eq. 6) is based on the spacing of discrete numbers of discontinuity sets. Both, spacing and the number of discontinuity sets are, however, ill-defined parameters and hard to assess in many practical geological scenarios: (i) discontinuity spacing defined as "the perpendicular distance between adjacent discontinuities" (ISO 14689) is geometrically only correctly measurable when discontinuity planes are perfectly parallel to each other and without variations of orientation. In reality, however, discontinuities are often neither parallel (e.g., Fig. 10a–c), nor have the same extent (e.g., Fig. 10e) or occur in folded rock masses where also fold planes are often not parallel (e.g., Fig. 10a, c; see also fold types after Ramsey (1967)—also given in Twiss and Moores (2007) chapter 10). In Fig. 10,

discontinuity spacing could only be reliably assessed for samples c, d and f, for some discontinuity sets with a well-defined orientation. ii) Whereas there are certainly many cases where a rock engineer can discriminate discrete discontinuity sets (e.g., massive and hard rock, few discontinuities, sedimentary rock masses with pronounced bedding planes), there are also many where it is not trivial to do so (e.g., many discontinuities, weak anisotropic rock masses, metamorphic rock masses, and folded rock masses). In these difficult cases, determining the number of occurring discontinuity sets is highly subjective which might be related to the fact that there is no definition of how a discontinuity set is quantitatively determined. Using the number of discontinuity sets as an input to calculate parameters such as J_{v5} (Eq. 6) or RQD/J_n in the Q-system ultimately leads to the extreme spread of values for these parameters which can be seen in Fig. 8 and also clustering of datapoints as can be seen in Fig. 9.

The use of parameters for rock mass structure characterization that are based on subjective estimations of the discontinuity spacing and/or the number of discontinuity sets is, therefore, discouraged for difficult geological settings as elaborated above. In contrast to J_{v1}, J_{v2} and J_{v5}, the proposed equations for J_{v3} (Eq. 4) and J_{v4} (Eq. 5) from Sonmez and Ulusay (1999) are based on measurable discontinuity frequencies which is seen as superior in terms of objectivity. However, since J_{v3} and J_{v4} compute the volumetric joint count as a product of its terms, the number of discontinuities increases exponentially with an increasing number of discontinuity intersections on a scanline and, therefore, these equations massively overestimate J_v and should not be used. The herein developed equation to estimate J_v (Eq. 31) is also based on objectively measurable discontinuity intersections while avoiding the problem of J_{v3} and J_{v4} and is, therefore, proposed as an improved replacement for all other J_v estimations.

RQD/J_n is the part of the Q-system that quantifies the structural complexity of the rock mass. With the use of J_n as a subjective parameter for the number of discontinuity sets in a rock mass, it suffers from the above-mentioned problems when it comes to discriminating individual discontinuity sets. Furthermore, the RQD—especially when it is estimated from exposures such as tunnel faces—is a highly ambiguous parameter and is not suitable as an input to rock mass classification schemes such as Q or RMR as elaborated in Pells et al. (2017).

Practical engineering should set a higher focus on the use of the *Pij* system (Dershowitz and Herda 1992) since this provides several parameters to objectively quantify the discontinuity density in rock masses. The author agrees with Dershowitz and Herda (1992) that $P32$ provides a scale- and orientation independent, isotropic quantification for the discontinuity density in rock masses that is superior to many others. While $P30/J_v$ is not as representative for the discontinuity density of a rock mass, it still provides a very useful estimation for that. Nevertheless, it is acknowledged that both $P32$ and $P30/J_v$ suffer from the problem of not being directly observable in practice. However, not only can Eq. 31 be used to estimate $P30/J_v$, great potential is also seen in the linear correlations between $P21$ and $P30/J_v$ (Eq. 11) and $P21$ and $P32$ (Eq. 12) that achieve high R^2 values of 0.99.

Parameters as the ones provided in the *Pij* system provide a more objective decision basis in rock engineering than "conventional" ones that are estimated by the onsite personnel and are subjected to their subjectivity and cognitive bias (Elmo and Stead 2021; Skretting et al. 2023). $P21$ (i.e., length of discontinuities per unit area) is objectively measurable and can be directly retrieved from images and scans of rock exposures. This is especially relevant in rock mechanical scenarios where a cut rock surface is at hand and scanning technology may be used for documentation: tunnel boring machine excavation (Gaich and Pötsch 2016), sawed rock cuts, cleanly blasted benches, rock surfaces created by road headers, etc.

5 Outlook

The obvious drawback and biggest potential for improvement of this study (and similar previous studies) is that the presented analyses and correlations are based on simulated discrete discontinuity networks. Therefore, the results of the study are limited to the extent of today's structural- and engineering geological understanding of the rock mass which PDD1 represents. A milestone will be reached once it is possible to set up a dataset such as PDD1 with real scans of rock masses at the outcrop scale and then develop parameters based on that. Today's technology (e.g., X-ray computed tomography) is limited to 3D scanning of laboratory scale samples and further developments are required to move this to the field scale as also discussed in Franzosi et al. (2023).

Nevertheless, the following improvements are under consideration for a future version of PDD1: (i) different modes of discontinuity termination; (ii) roughness on multiple scales for individual discontinuities; (iii) discontinuity models including an aperture/volume thus enabling measuring volumetric parameters of the *Pij* system: $P11$ (discontinuity length per unit length), $P22$ (discontinuity area per unit area), $P33$ (discontinuity volume per unit volume). These developments, however, heavily impact the computational demand to both generate samples and also perform virtual measurements on them. Increasing the overall sample size from the current $10 \times 10 \times 10$ m would be desirable but poses the same

computational challenge if the high discontinuity density of PDD1 is to be maintained.

Even though PDD1 was designed to comprise as many different rock mass structures as possible, no dataset is ever all encompassing and unbiased. Just as the relationship between RQD and $P10$ (Eq. 29) from Priest and Hudson (1976) was verified through PDD1, it is encouraged that future studies investigate the validity of the herein proposed relationships based on virtual discontinuity networks that were created by other means.

Besides increasing the realism of the dataset, future developments shall also comprise more sophisticated analyses. While the *Pij* parameters are seen as state-of-the-art for characterizing the discontinuity density of a rock mass, there is room for improvement and, for example, there is no parameter today that considers structural rock mass anisotropy which can be decisive for rock engineering. In early phases of this study, it was also attempted to use PDD1 to directly characterize the block system that results from the modeled intersections between discontinuities. While the rock mechanical relevance of block properties is undoubted, this line of investigation was discontinued for PDD1 due to computational problems related to high discontinuity densities and folded discontinuities. A future version of the study shall dive deeper into blocks resulting from intersections between discontinuities. It is also highlighted that that the herein proposed relationships cover a large range of discontinuity densities going from very low to extremely high ones. The relationships are, therefore, robust with respect to this large range but could be refined for more narrow ranges of low, intermediate or high discontinuity densities depending on the geology of interest. Given that all analyses of PDD1 are provided as supplementary material, investigating more specific relationships for narrower ranges of discontinuity densities can easily be done by future studies.

Studying rock mass structure based on state-of-the-art discrete discontinuity networks has the potential to revise and improve rock mass characterization parameters that have been developed decades ago. This study should, however, not only revise already existing methods, but pave the way for future methods of rock mass characterization. Ultimately, the goal of ground characterization is to quantify ground properties as close to reality as possible to enable an engineering design that is as fitting as possible.

Appendix

See Tables 5, 6, 7, 8, 9.

Table 5 Overview of all parameters of the parametric discontinuity dataset 1 (PDD1). Types: i … input, m … measured, c … computed. See Table 1 for definition of the P_{ij} notation

Type	Parameter name	Definition	References
i	Identifier	Unique identifier for each sample	
i	Bounding box size [m]	Edge size of the samples' bounding boxes	
i	Jv boxes edge size [m]	Edge size of one "unit volume" of rock mass	ISO 14689
i	Seed	Random seed to reproduce the stochastic elements of the dataset	
i	Set 1—n joints	Number of finite and planar discontinuities of set 1	
i	Set 1—radius [m]	Mean radius of finite and planar discontinuities of set 1	
i	Set 1—radius std [m]	Standard deviation of the radius of finite and planar discontinuities of set 1	
i	Set 1—dip direction [°]	Mean dip direction of finite and planar discontinuities of set 1	ISO 14689
i	Set 1—dip direction std [°]	Standard deviation of the dip direction of finite and planar discontinuities of set 1	
i	Set 1—dip [°]	Mean dip of finite and planar discontinuities of set 1	ISO 14689
i	Set 1—dip std [°]	Standard deviation of the dip of finite and planar discontinuities of set 1	
i	Set 1—type	Type of discontinuity set 1: 0 = planar and finite, 1 = folded and persistent	
i	F_rand_sin	Multiplication factor for the sinus function that generates a folded set 1	
i	F_rand_n_planes	Number of folded set 1 discontinuity planes	
i	F_rand_angle	Random angle to rotate the folded set 1 around an axis	
i	F_rand_axis_x	x-component of the rotation axis to rotate the folded set 1	
i	F_rand_axis_y	y-component of the rotation axis to rotate the folded set 1	
i	F_rand_axis_z	z-component of the rotation axis to rotate the folded set 1	
i	Set 2—n joints	Number of finite and planar discontinuities of set 2	
i	Set 2—radius [m]	Mean radius of finite and planar discontinuities of set 2	
i	Set 2—radius std [m]	Standard deviation of the radius of finite and planar discontinuities of set 2	
i	Set 2—dip direction [°]	Mean dip direction of finite and planar discontinuities of set 2	ISO 14689
i	Set 2—dip direction std [°]	Standard deviation of the dip direction of finite and planar discontinuities of set 2	
i	Set 2—dip [°]	Mean dip of finite and planar discontinuities of set 2	ISO 14689
i	Set 2—dip std [°]	Standard deviation of the dip of finite and planar discontinuities of set 2	
i	Set 3—n joints	Number of finite and planar discontinuities of set 3	
i	Set 3—radius [m]	Mean radius of finite and planar discontinuities of set 3	
i	Set 3—radius std [m]	Standard deviation of the radius of finite and planar discontinuities of set 3	
i	Set 3—dip direction [°]	Mean dip direction of finite and planar discontinuities of set 3	ISO 14689
i	Set 3—dip direction std [°]	Standard deviation of the dip direction of finite and planar discontinuities of set 3	
i	Set 3—dip [°]	Mean dip of finite and planar discontinuities of set 3	ISO 14689
i	Set 3—dip std [°]	Standard deviation of the dip of finite and planar discontinuities of set 3	
i	Random set—n joints	Number of random discontinuities in set 4	
i	Random set—radius [m]	Mean radius of random discontinuities in set 4	
i	Random set—radius std [m]	Standard deviation of random discontinuities in set 4	
m	Meas. spacing set 1 [m]	Normal spacing of discontinuity set 1	
m	Meas. spacing set 2 [m]	Normal spacing of discontinuity set 2	
m	Meas. spacing set 3 [m]	Normal spacing of discontinuity set 3	
m	RQD Y	RQD along a measuring line parallel to the global Y-axis	ISO 14689
m	RQD X	RQD along a measuring line parallel to the global X-axis	ISO 14689
m	RQD Z	RQD along a measuring line parallel to the global Z-axis	ISO 14689
m	Apparent spacing Y [m]	Average length of the pieces of a measuring line parallel to the global Y-axis intersected by all discontinuities	

Table 5 (continued)

Type	Parameter name	Definition	References
m	Apparent spacing X [m]	Average length of the pieces of a measuring line parallel to the global X-axis intersected by all discontinuities	
m	Apparent spacing Z [m]	Average length of the pieces of a measuring line parallel to the global Z-axis intersected by all discontinuities	
m	P10 Y	P10 along a measuring line parallel to the global Y-axis	Dershowitz and Herda (1992)
m	P10 X	P10 along a measuring line parallel to the global X-axis	Dershowitz and Herda (1992)
m	P10 Z	P10 along a measuring line parallel to the global Z-axis	Dershowitz and Herda (1992)
m	P20 X	P20 measured in a plane perpendicular to the global X-axis	Dershowitz and Herda (1992)
m	P21 X	P21 measured in a plane perpendicular to the global X-axis	Dershowitz and Herda (1992)
m	P20 Y	P20 measured in a plane perpendicular to the global Y-axis	Dershowitz and Herda (1992)
m	P21 Y	P21 measured in a plane perpendicular to the global Y-axis	Dershowitz and Herda (1992)
m	P20 Z	P20 measured in a plane perpendicular to the global Z-axis	Dershowitz and Herda (1992)
m	P21 Z	P21 measured in a plane perpendicular to the global Z-axis	Dershowitz and Herda (1992)
m	Jv measured [discs/m^3]	Number of discontinuities in a unit volume of 1 m3 of rock mass	ISO 14689
m	P32	Sum of the discontinuity area per unit volume (1 m3) of rock mass	Dershowitz and Herda (1992)
m	Set 1 total area [m2]	Total area of discontinuity set 1	
m	Set 2 total area [m2]	Total area of discontinuity set 2	
m	Set 3 total area [m2]	Total area of discontinuity set 3	
m	Random set total area [m2]	Total area of the random discontinuity set	
m	Minkowski dimension	Fractal dimension of the sample computed acc. to Minkowski–Bouligand– also known as "box counting dimension"	
c	Avg. P10	Average value of P10 parallel to the X, Y and Z directions	
c	Avg. P20	Average value of P20 parallel to the X, Y and Z directions	
c	Avg. P21	Average value of P21 parallel to the X, Y and Z directions	
c	Avg. app. spacing [m]	Average value of the apparent spacing parallel to the X, Y and Z directions	
c	Avg. RQD	Average value of the RQD parallel to the X, Y and Z directions	
c	Jv ISO 14689 (2019)	Computed volumetric joint count	ISO 14689, Palmstrøm (1982)
c	Jv Palmstrøm (2000)	Computed volumetric joint count	Palmstrøm (2000)
c	Jv Sonmez and Ulusay (1999) 1	Computed volumetric joint count	Sonmez and Ulusay (1999)
c	Jv Sonmez and Ulusay (1999) 2	Computed volumetric joint count	Sonmez and Ulusay (1999)
c	Jv Erharter (2023)	Computed volumetric joint count	Equation 31
c	Tot disc. area [m2]	Sum of measured, total areas of discontinuity sets 1–4	
c	Set_1_ratio	Ratio of the total area of discontinuity set 1 to the total discontinuity area	
c	Set_2_ratio	Ratio of the total area of discontinuity set 2 to the total discontinuity area	
c	Set_3_ratio	Ratio of the total area of discontinuity set 3 to the total discontinuity area	
c	Rand_set_ratio	Ratio of the total area of discontinuity set 4 to the total discontinuity area	
c	n_discs	Computed number of discontinuities based on the discontinuity area ratios	
c	Qsys_Jn	Computed "joint number" of the "Q-system" based on the discontinuity area ratios	
c	Q_struct	Term of the Q-system that refers to the rock mass structure (i.e. RQD/Jn)	See, e.g., Barton et al. (1974)
c	Avg. disc. set spacing [m]	Average value of the measured spacing of discontinuity sets 1, 2 and 3	
c	Jv Sonmez and Ulusay (2002)	Computed volumetric joint count	Sönmez and Ulusay (2002)
c	Alpha [°]	Angle between discontinuity sets 1 and 2	

Table 5 (continued)

Type	Parameter name	Definition	References
c	Beta [°]	Angle between discontinuity sets 1 and 3	
c	Gamma [°]	Angle between discontinuity sets 2 and 3	
c	Block volume computed [m^3]	Computed volume of rock blocks	Palmstrøm (2000)

Table 6 Statistical values of input parameters of PDD1 for samples with planar discontinuities only

Parameter	Count	Mean	Std	Min	25%	50%	75%	Max
Set 1—n joints	2462	194.805	115.4158	0	93	192	296	400
Set 1—radius [m]	2450	4.020249	2.230843	0.256552	2.089881	3.867828	5.993466	7.99998
Set 1—radius std [m]	2462	1.000357	0.855856	0.00037	0.302019	0.759629	1.469955	3.939842
Set 1—dip direction [°]	2450	183.2624	105.9587	0	92	186	275	360
Set 1—dip direction std [°]	2462	19.87855	11.91809	0	9	20	30	40
Set 1—dip [°]	2450	44.98531	25.88196	0	23	45	67	90
Set 1—dip std [°]	2462	9.932169	6.02722	0	5	10	15	20
Set 2—n joints	2462	196.0471	116.131	0	92	192	298	400
Set 2—radius [m]	2457	4.115612	2.179891	0.256502	2.209197	4.092712	5.999529	7.998077
Set 2—radius std [m]	2462	1.062086	0.87567	0.001216	0.343647	0.837825	1.570756	3.934399
Set 2—dip direction [°]	2457	178.9341	103.7641	0	88	178	268	360
Set 2—dip direction std [°]	2462	19.96669	11.90695	0	10	20	30	40
Set 2—dip [°]	2457	44.53439	26.72307	0	21	44	68	90
Set 2—dip std [°]	2462	9.987002	6.092394	0	5	10	15	20
Set 3—n joints	2462	192.524	117.0165	0	89	190	296	400
Set 3—radius [m]	2459	4.045161	2.20559	0.254065	2.08373	3.928015	5.90328	7.990568
Set 3—radius std [m]	2462	1.035504	0.881338	0.000311	0.302917	0.780493	1.588583	3.929726
Set 3—dip direction [°]	2459	179.4229	104.8652	0	86	182	272	360
Set 3—dip direction std [°]	2462	19.91024	11.85482	0	10	20	30	40
Set 3—dip [°]	2459	45.20984	27.04208	0	21	45	69	90
Set 3—dip std [°]	2462	9.956539	6.041518	0	5	10	15	20
Random set—n joints	2462	196.4797	115.3168	0	94.25	195.5	298.75	400
Random set—radius [m]	2458	2.030268	0.663688	0.266459	1.553352	2.046738	2.498195	3.877368
Random set—radius std [m]	2462	0.50656	0.356901	0.000596	0.207859	0.447515	0.745598	1.656139
Bounding box size [m]	2462	10	0	10	10	10	10	10
Jv boxes edge size [m]	2462	1	0	1	1	1	1	1

Table 7 Statistical values of input parameters of PDD1 for samples with folded and planar discontinuities

Parameter	Count	Mean	Std	Min	25%	50%	75%	Max
F_rand_sin	2538	0.99263	0.582297	0.001213	0.480209	0.983603	1.5013	1.997937
F_rand_n_planes	2538	181.4015	68.84734	60	124	184	241	300
F_rand_angle	2538	178.2284	103.5505	0.382115	89.34803	178.7819	267.6433	359.546
F_rand_axis_x	2538	0.509878	0.29203	0.001414	0.260387	0.505859	0.772703	0.999642
F_rand_axis_y	2538	0.499836	0.289153	4.55E-06	0.255001	0.498256	0.744122	0.999756
F_rand_axis_z	2538	0.500944	0.289627	0.000163	0.255033	0.503304	0.751855	0.999668
Set 2—n joints	2538	193.1312	116.5869	0	89	191	293	400
Set 2—radius [m]	2533	4.025295	2.200442	0.264024	2.12592	3.902147	5.889822	7.999471
Set 2—radius std [m]	2538	1.000831	0.863749	0.00031	0.314388	0.74946	1.490847	3.935678
Set 2—dip direction [°]	2533	180.9755	104.8291	0	91	180	271	360
Set 2—dip direction std [°]	2538	20.00788	11.90277	0	10	20	30	40
Set 2—dip [°]	2533	45.02842	26.74628	0	21	46	68	90
Set 2—dip std [°]	2538	10.03113	6.015698	0	5	10	15	20
Set 3—n joints	2538	195.6233	118.1626	0	91	193	298	400
Set 3—radius [m]	2531	4.132287	2.237464	0.255176	2.230495	4.027359	6.082117	7.999803
Set 3—radius std [m]	2538	1.022038	0.868253	0.000774	0.312785	0.778834	1.505768	3.8526
Set 3—dip direction [°]	2531	179.9226	104.3564	0	89	182	272	360
Set 3—dip direction std [°]	2538	19.94602	11.96002	0	9	20	30	40
Set 3—dip [°]	2531	44.88226	26.8185	0	22	44	69	90
Set 3—dip std [°]	2538	9.899921	6.072567	0	5	10	15	20
Random set—n joints	2538	195.238	117.4551	0	89.25	192.5	299	400
Random set—radius [m]	2529	2.025761	0.662502	0.292568	1.557392	2.04778	2.496375	3.801486
Random set—radius std [m]	2538	0.505718	0.350288	0.000579	0.222364	0.446896	0.738765	1.735004
Bounding box size [m]	2538	10	0	10	10	10	10	10
Jv boxes edge size [m]	2538	1	0	1	1	1	1	1

Table 8 Statistical values of measured parameters of PDD1

Parameter	Count	Mean	Std	Min	25% percentile	Median	75% percentile	Max
Meas. spacing set 1 [m]	4930	0.58	0.87	0.03	0.20	0.34	0.59	8.25
Meas. spacing set 2 [m]	4890	0.68	1.21	0.03	0.08	0.19	0.63	7.67
Meas. spacing set 3 [m]	4888	0.72	1.27	0.03	0.08	0.18	0.65	8.15
RQD Y	5000	71.52	23.65	1.62	55.29	77.21	92.21	100.00
RQD X	5000	71.85	23.82	1.24	55.66	77.81	92.44	100.00
RQD Z	5000	55.45	29.31	0.00	30.00	56.14	82.57	100.00
Apparent spacing Y [m]	4994	0.21	0.36	0.02	0.07	0.11	0.21	5.00
Apparent spacing X [m]	4993	0.22	0.36	0.02	0.07	0.11	0.22	5.00
Apparent spacing Z [m]	4997	0.13	0.25	0.01	0.04	0.07	0.13	5.00
P10 Y	5000	10.79	8.04	0.00	4.60	8.90	15.10	51.40
P10 X	5000	10.73	8.15	0.00	4.40	8.70	15.10	51.80
P10 Z	5000	17.21	12.13	0.00	7.40	14.80	24.33	77.00
P20 X	5000	3.59	1.78	0.10	2.25	3.48	4.77	11.56
P21 X	5000	19.66	12.29	0.05	9.82	18.11	27.47	78.05
P20 Y	5000	3.58	1.78	0.06	2.24	3.49	4.75	10.35
P21 Y	5000	19.63	12.32	0.04	9.77	18.05	27.50	72.48
P20 Z	5000	2.72	1.47	0.07	1.60	2.56	3.67	9.13
P21 Z	5000	14.63	9.88	0.07	6.77	12.64	20.79	62.91
Jv measured [discs/m^3]	5000	33.84	18.72	0.53	19.28	31.96	46.13	117.16
P32	5000	20.20	11.98	0.10	10.75	18.84	28.04	71.77
Set 1 total area [m2]	5000	4666.39	5098.18	0.00	1644.31	3042.42	4846.38	28,817.60
Set 2 total area [m2]	5000	6619.12	6596.49	0.00	1206.49	4334.78	10,413.71	30,745.98
Set 3 total area [m2]	5000	6680.73	6693.31	0.00	1128.57	4369.50	10,525.92	29,867.96
Random set total area [m2]	5000	2228.93	1894.92	0.00	685.06	1782.10	3321.49	10,875.48
Minkowski dimension	5000	2.41	0.25	1.55	2.24	2.45	2.60	2.90

Table 9 Statistical values of computed parameters of PDD1

Parameter	Count	Mean	Std	Min	25% percentile	Median	75% percentile	Max
Avg. P10	5000	12.91	8.04	0.03	6.43	11.93	18.14	48.77
Avg. P20	5000	3.30	1.59	0.08	2.11	3.22	4.36	9.60
Avg. P21	5000	17.97	10.89	0.05	9.24	16.79	25.04	65.90
Avg. app. spacing [m]	4987	0.18	0.27	0.02	0.06	0.10	0.19	3.61
Avg. RQD	5000	66.27	22.02	5.35	49.42	67.42	85.35	100.00
Jv ISO 14689 (2019)	5000	21.11	13.22	0.00	10.58	19.50	29.53	77.97
Jv Palmstrøm (2000)	5000	21.31	13.22	0.20	10.78	19.70	29.73	78.17
Jv Sonmez and Ulusay (1999) 1	5000	4076.68	7589.81	0.00	191.63	1183.25	4676.04	114,993.93
Jv Sonmez and Ulusay (1999) 2	5000	5000.02	8707.12	0.00	266.26	1699.36	5970.80	115,976.29
Jv Erharter (2023)	5000	32.98	19.29	2.08	17.44	30.64	45.54	119.04
Tot disc. area [m^2]	5000	20,195.18	11,981.49	97.27	10,750.58	18,836.96	28,043.39	71,770.85
set_1_ratio	5000	0.26	0.21	0.00	0.09	0.19	0.37	0.98
set_2_ratio	5000	0.31	0.23	0.00	0.10	0.27	0.48	0.97
set_3_ratio	5000	0.31	0.24	0.00	0.10	0.27	0.49	0.96
rand_set_ratio	5000	0.12	0.10	0.00	0.05	0.10	0.16	0.87
n_discs	5000	1.82	0.81	0.00	1.00	2.00	2.00	4.00
Qsys_Jn	5000	5.27	5.34	1.00	2.00	4.00	4.00	20.00
Q_struct	5000	22.56	13.70	0.27	11.76	22.03	32.64	100.00
Avg. disc. set spacing [m]	4999	0.67	0.71	0.04	0.21	0.38	0.85	7.12
Jv Sonmez & Ulusay (2002)	4999	7.09	8.78	0.00	1.70	4.04	9.12	73.92
Alpha [°]	2445	72.78	26.85	12.51	53.52	71.21	89.88	164.22
Beta [°]	2447	72.29	27.56	11.00	52.08	71.66	89.99	160.96
Gamma [°]	4980	71.98	27.66	11.00	52.47	70.61	88.97	167.00
Block volume computed [m^3]	2307	0.26	1.64	0.00	0.00	0.01	0.04	46.93

See Fig. 11.

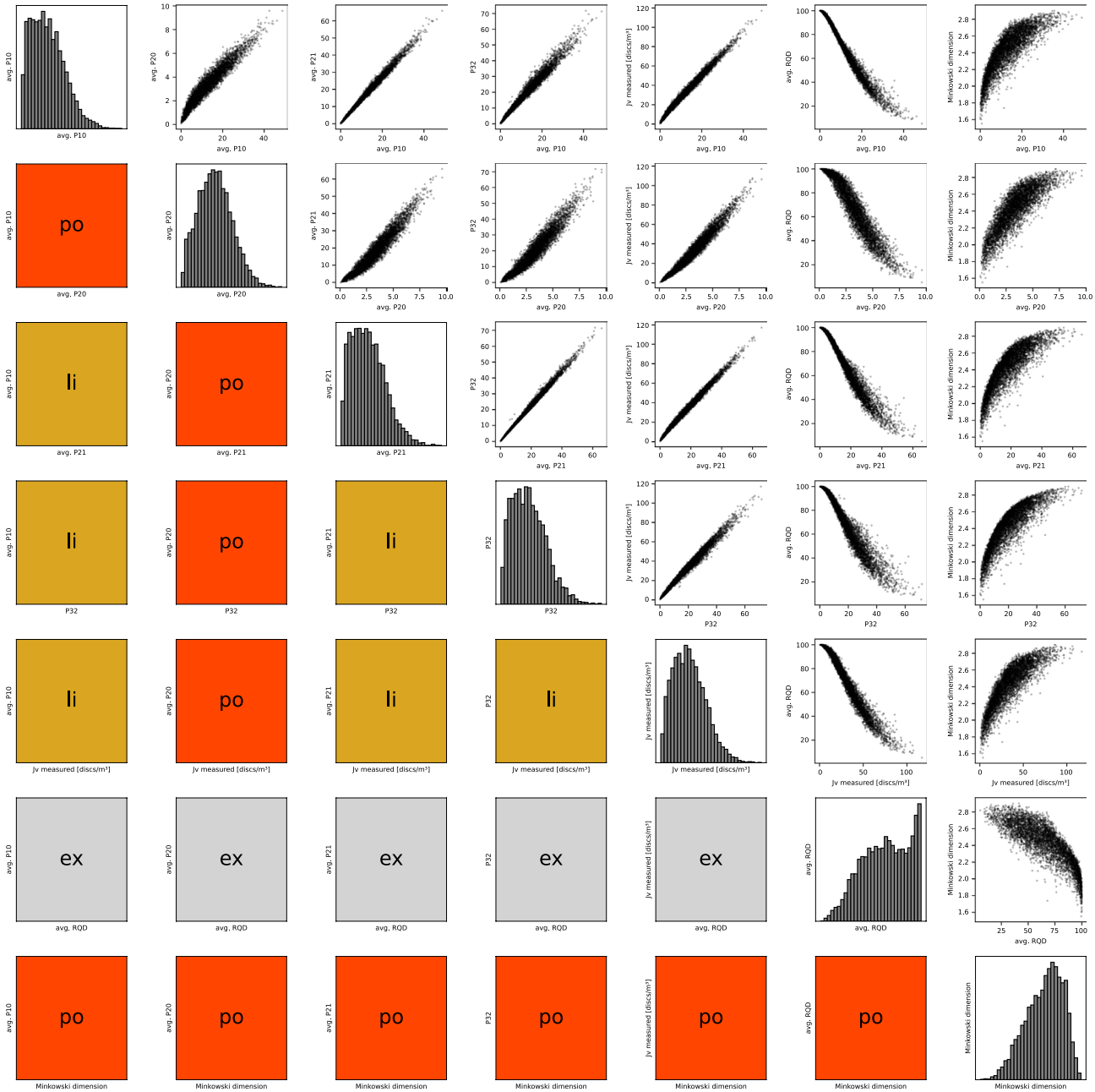

Fig. 11 Pairplot showing relationships of different parameters of PDD1. Above the diagonal, scatterplots of relationships are shown, below the diagonal, the type of relationship is indicated: *li* linear, *po* power law, *ex* exponential; the diagonal shows histograms of the individual parameters. The reader is referred to the online version of the article for the high-resolution version of this figure

Acknowledgements The efforts for proofreading this manuscript by Jessica Ka Yi Chiu (NGI) are highly acknowledged.

Funding Open access funding provided by Norwegian Geotechnical Institute. Open access funding provided by Norwegian Geotechnical Institute.

Data availability The parametric discontinuity dataset 1 (PDD1), Grasshopper scripts for generating the dataset and Python codes for data compilation and analyses can be found under this Github Link: https://github.com/geograz/Parametric_Rockmass_Studies/releases/tag/v1.0.0.

Conflict of Interest
The author declares no conflicts of interest.

References

Barton N, Lien R, Lunde J (1974) Engineering classification of rock masses for the design of tunnel support. Rock Mech 6:189–236. https://doi.org/10.1007/BF01239496

Berkowitz B, Hadad A (1997) Fractal and multifractal measures of natural and synthetic fracture networks. Journal of Geophysical Research 102

Bieniawski ZT (1973) Engineering classification of jointed rock masses. Civ Eng South Afr 1973(12):335–343

Boadu FK, Long LT (1994) The fractal character of fracture spacing and RQD. Int J Rock Mech Min Sci Geomech Abstr 31:127–134. https://doi.org/10.1016/0148-9062(94)92802-9

Deere DU (1964) Technical description of rock cores for engineering purpose. Rock Mech Eng Geol 1(1):16–22

Dershowitz WS, Herda HH (1992) Interpretation of fracture spacing and intensity. In: Tillerson JR, Wawersik WR (eds) Rock mechanics: Proceedings of the 33rd US symposium. Netherlands: AA Balkema

Elmo D, Stead D (2021) The role of behavioural factors and cognitive biases in rock engineering. Rock Mech Rock Eng 54:2109–2128. https://doi.org/10.1007/s00603-021-02385-3

Franzosi F, Casiraghi S, Colombo R, Crippa C, Agliardi F (2023) Quantitative evaluation of the fracturing state of crystalline rocks using infrared thermography. Rock Mech Rock Eng. https://doi.org/10.1007/s00603-023-03389-x

Gaich A, Pötsch M (2016) 3D images for digital tunnel face documentation at TBM headings - application at Koralmtunnel lot KAT2 / 3D-Bilder zur digitalen Ortsbrustdokumentation bei TBM- Vortrieben - Anwendung beim Koralmtunnel Baulos KAT2. Geomech Tunnelbau 9:210–221. https://doi.org/10.1002/geot.201600018

Gómez S, Sanchidrián JA, Segarra P, Bernardini M (2023) A non-parametric discrete fracture network model. Rock Mech Rock Eng 56:3255–3278. https://doi.org/10.1007/s00603-022-03194-y

Hoek E (1999) Putting numbers to geology–an engineer's viewpoint. Q J Eng GeolHydrogeol 32:1–19. https://doi.org/10.1144/GSL.QJEG.1999.032.P1.01

Lee Y-H, Carr JR, Barr DJ, Haas CJ (1990) The fractal dimension as a measure of the roughness of rock discontinuity profiles. Int J Rock Mech Min Sci Geomech Abstr 27:453–464. https://doi.org/10.1016/0148-9062(90)90998-H

NS-EN ISO 14689:2018 (2018) Geotechnical investigation and testing Identification, description and classification of rock. Standard Norge

Ojeda P, Elmo D, Rogers S, Brzovic A (2023) Discrete fracture network (DFN) analysis to quantify the reliability of borehole-derived volumetric fracture intensity. Geosciences 13:187. https://doi.org/10.3390/geosciences13060187

Palmstrøm A (1974) Characterization of jointing density and the quality of rock masses

Palmstrøm A (1982) The volumetric joint count - a useful and simple measure of the degree of rock mass jointing. In: IV Congress International Association of Engineering Geology, vol. 2. pp 221–228

Palmstrøm A (1995) RMi-A rock mass characterization system for rock engineering purposes. Ph.D. thesis, University of Oslo

Palmstrøm A (1996) Characterizing rock masses by the RMi for use in practical rock engineering. Tunn Undergr Space Technol 11:175–188. https://doi.org/10.1016/0886-7798(96)00015-6

Palmstrøm A (2000) Block Size and Block Size Distribution. In: GeoEng2000 conference

Palmstrøm A (2005) Measurements of and correlations between block size and rock quality designation (RQD). Tunn Undergr Space Technol 20:362–377. https://doi.org/10.1016/j.tust.2005.01.005

Pells PJ, Bieniawski ZT, Hencher SR, Pells SE (2017) Rock quality designation (RQD): time to rest in peace. Can Geotech J 54:825–834. https://doi.org/10.1139/cgj-2016-0012

Priest SD, Hudson JA (1976) Discontinuity spacings in rock. Int J Rock Mech Min Sci Geomech Abstr 13:A91. https://doi.org/10.1016/0148-9062(76)91605-3

Ramsey JG (1967) Folding and fracturing of rocks. Open J Geol 6

Robert McNeel & Associates (2023) Rhino. https://www.rhino3d.com/

Rogers S, Bewick R, Brzovic A, Gaudreau D (2017) Integrating photogrammetry and discrete fracture network modelling for improved conditional simulation of underground wedge stability. In: Proceedings of the Eighth International Conference on Deep and High Stress Mining. Australian Centre for Geomechanics, Perth, pp 599–610

Roy A, Perfect E, Dunne WM, McKay LD (2007) Fractal characterization of fracture networks: an improved box-counting technique. J Geophys Res. https://doi.org/10.1029/2006JB004582

Skretting E, Erharter GH, Chiu JKY (2023) Virtual reality based uncertainty assessment of rock mass characterization of tunnel faces. In: Schubert W, Kluckner A (eds) Proceedings of the 15th ISRM Congress 2023 & 72nd Geomechanics Colloquium: Challenges in Rock Mechanics and Rock Engineering

Sonmez H, Ulusay R (1999) Modifications to the geological strength index (GSI) and their applicability to stability of slopes. Int J Rock Mech Min Sci 36:743–760. https://doi.org/10.1016/S0148-9062(99)00043-1

Sönmez H, Ulusay R (2002) A discussion on the Hoek–Brown failure criterion and suggested modifications to the criterion verified by slope stability case studies. Yerbilimleri 26:77–99

Terzaghi K (1946) Rock defects and loads on tunnel supports: introduction to rock tunnelling with steel supports. Harvard University, Cambridge, p 95

Twiss RJ, Moores EM (2007) Structural geology, 2nd edn. Freeman, New York

Ulusay R, Hudson JA (eds) (2007) The complete ISRM suggested methods for rock characterization, testing and monitoring: 1974–2006, vol 15. International Soc. for Rock Mechanics, Commission on Testing Methods, Ankara

Xiao K, Zhang R, Xie J, Ren L, Gao M, Zhang Z, Lou C, Ai T, Zha E (2023) Analytical solutions for the characteristic size distribution of the elliptical model in fractured rock mass. Rock Mech Rock Eng 56:3927–3948. https://doi.org/10.1007/s00603-023-03263-w

Zhang L (2016) Determination and applications of rock quality designation (RQD). J Rock Mech Geotech Eng 8:389–397. https://doi.org/10.1016/j.jrmge.2015.11.008

Zhang Q, Wang X, Zhu H, Zhang K, Li X (2022) Mixture distribution model for three-dimensional geometric attributes of

multiple discontinuity sets based on trace data of rock mass. Eng Geol 311:106915. https://doi.org/10.1016/j.enggeo.2022.106915

Zheng J, Wang X, Lü Q, Liu J, Guo J, Liu T, Deng J (2020) A Contribution to relationship between volumetric joint count (Jv) and rock quality designation (RQD) in three-dimensional (3-D) space. Rock Mech Rock Eng 53:1485–1494. https://doi.org/10.1007/s00603-019-01986-3